Regional Studies in Marine Science 64 (2023) 103054

Contents lists available at ScienceDirect

Regional Studies in Marine Science

journal homepage: www.elsevier.com/locate/rsma

A fjord with a land-terminating glacier: Meltwater, bio-optics, particulate matter, nutrients, phytoplankton species, and primary production in west Greenland

Lars Chresten Lund-Hansen [a,*], Ingela Dahllöf [b], Morten Holtegaard Nielsen [c]

[a] Arctic Research Center, Aquatic Biology, Department of Biology, Aarhus University, Denmark
[b] Biological & Environmental Sciences, University of Gothenburg, Sweden
[c] Marine Science and Consulting, Copenhagen, Denmark

ARTICLE INFO

Article history:
Received 14 October 2022
Received in revised form 30 May 2023
Accepted 12 June 2023
Available online 16 June 2023

Keywords:
Land-terminating glacial fjord
Meltwater
Bio-optical properties
Particulate matter
Nutrients
Primary production
Greenland

ABSTRACT

Land-terminating glaciers and submarine melting of marine-terminating glaciers are significant features in Arctic regions and are foreseen to become more frequent as marine-terminating glaciers ultimately develop into a land-terminated state. A transition driven by the continuous rise in Arctic air temperatures, and emphasizes the importance of studies of land-terminating glaciers their bio-optical properties and biogeochemistry. Kangerlussuaq in west Greenland with a land-terminating glaciers and was selected for this study. During a research cruise we measured spectral and PAR attenuation, particulate matter concentrations, salinity, nutrient concentrations, Chl*a*, and phytoplankton species composition, along a transect from river outlet to open marine waters. Results showed that surface waters in Kangerlussuaq were strongly influenced by meltwater with low salinities, high particulate matter concentrations, high PAR and spectral light attenuation coefficients, and low nutrient concentrations. Spectral composition was also affected by the particulate matter. PAR photic depths varied between 4 and 9 m dependent on particulate matter concentrations. There was a decrease with distance from outlet in silicate concentrations, and opposite for phosphate, which increased significantly from river outlet to the marine. Phytoplankton species number (42) and diversity were high at the marine station but low (3) in turbid waters dominated by the diatom *Skeletonema costatum* in high numbers. A meltwater plume covered about 50 % of the Kangerlussuaq at average discharges in early August. Primary production was quantified with a simple model based on light attenuation coefficients, and showed a near exponential decrease in production with increase in attenuation.

1. Introduction

Rising air temperatures in the Arctic (Box et al., 2019) are enhancing the melting of the Greenland Ice Sheet (GrIS) (Young et al., 2022), which also enhances the submarine melting of marine-terminating glaciers (Straneo and Heimbach, 2013). This melting increases the freshwater discharges from the glaciers into the receiving fjords both for marine-terminating (Cook et al., 2019) and land-terminating glaciers (Stuart-Lee et al., 2021). There has been some focus on marine-terminating glaciers and their related biogeochemistry (Halbach et al., 2019), and also in a trophic context (Hopwood et al., 2020; Vonnahme et al., 2021) as some are hot spots of increased primary production (Meire et al., 2017). Marine-terminating glaciers alter and change the circulation pattern in the receiving fjord (Gillard et al., 2016). However, a significant number of marine-terminating glaciers ae likely to develop into land-terminating glaciers, with the continuous retreat of glaciers related to the greatly amplified increase in air temperatures in the Arctic (Huang et al., 2017). Advection of warmer waters into the fjords with marine-terminating glaciers also drives ice melting (Wood et al., 2021). Land-terminating glaciers and fjords that receive meltwater with high particulate matter are significant features in the Canadian Arctic (Kienholz et al., 2015), Svalbard (Möller et al., 2016), Patagonia (Davies and Glasser, 2017), New Zealand (Eaves et al., 2017), Antarctica (Rosa et al., 2020), and Greenland, with more than 35 land-terminating glaciers on Greenland's west coast (Meire et al., 2017).

Meltwater discharge from a glacier is strongly variable over time within a year, but high discharges are generally linked to increased melting of the glacier (Straneo and Cenedese, 2015). With increased discharges, more sediment particles will be transported in suspension with the meltwater (Cantoni et al., 2020). Sudden glacial peak flows induced by increased subglacial discharges (Straneo and Heimbach, 2013) and glacial lake breaching

* Corresponding author.
E-mail address: lund-hansen@bio.au.dk (L.C. Lund-Hansen).

https://doi.org/10.1016/j.rsma.2023.103054

(Mayer and Schuler, 2005; Mernild and Hasholt, 2009) also imply high discharges and increased sediment transport in glacial rivers (Crumley et al., 2017). Not only the receiving fjords, but also coastal waters and shelf areas, are influenced by the meltwater. For example, there is a significant glacier-derived meltwater-mediated transport of particulate matter to the shelf areas of Greenland (Overeem et al., 2017). Apparently, this meltwater with nutrients and iron specifically has sustained and added to the primary production on the Greenland shelf (Arrigo et al., 2017). Conversely, in a west Greenland study most of the iron was assimilated inside the fjord, rather than being exported to the shelf (Hopwood et al., 2016). Some fjord and estuary studies have found increased particulate matter and strong light attenuation in the water can effectively reduce the primary production (Cloern, 1987; Retamal et al., 2007; Gameiro et al., 2011), with light and nutrients as the main factors limiting photosynthesis (Falkowski and Raven, 2007). Here, secondary production and zooplankton reproduction was negatively affected by increased particulate matter (Arndt et al., 2011), which will also pose difficulties for vision-based foraging organisms such as fish (Aksnes et al., 2004) and birds (Nishizawa et al., 2020).

In this study we present data on salinity, light attenuation both for PAR (Photosynthetically Active Radiation) and spectrally resolved irradiance, particulate matter, nutrients, chlorophyll-*a* (Chl*a*) and phytoplankton species composition along a transect in Kangerlussuaq Fjord, which is strongly influenced by meltwater discharges from land-terminating glaciers, during August 2007. The main questions addressed here are: (1) How does meltwater with particulate matter at various concentrations affect optical properties in terms of the attenuation coefficients for K_d(PAR) and spectrally resolved $K_d(\lambda)$? (2) How do photic depths in the water column vary at various particulate matter concentrations? (3) Particulate matter is known to inhibit primary production, but can this relation be quantified? (4) What are the nutrient concentrations at this stage in late summer, and are there any gradients between the river outlet and the open ocean? (5) Are there any differences in phytoplankton species composition, number of cells, and diversity in relations to meltwater particulate matter concentrations? (6) What is the thickness of the meltwater plume and approximately how large is the area of the fjord covered by the plume?

2. Materials and methods

2.1. Study area and data collection

Kangerlussuaq Fjord on the west coast of Greenland is about 180 km long and varies in width from 5 to 6 km in its inner part to 1 to 2 km in its outer part with a total surface area of about 490 km^2 (Fig. 1). A shallow (30–40 m) sill extends about 90 km from the entrance of the fjord and inwards, after which water depths increase and reach up to 280 m in the central part. It has a diurnal tide and a spring tidal range of about 3 m (Nielsen et al., 2010). Kangerlussuaq Fjord receives meltwater from the Greenland Ice Sheet (GrIS) via the Watson and Umivit Rivers, with a contribution from the Sarfartoq River (Fig. 1).

Total annual average discharge volumes between 2007–2010 reached 3.5 km^3, and total suspended particulate matter (SPM) transport was 7.3 $\times$ 10^6 tons in the Watson River as an average summer melt season comprising the years 2007–2010 (Hasholt et al., 2012). The freshwater discharge to the fjord takes place only from early May to early September, with sea ice development in late November or early December (Lund-Hansen et al., 2014). Discharges and SPM transport in the Umivit and Sarfartoq Rivers are unknown (Hudson et al., 2014).

2.2. CTD, optical sensors, and optical data processing

Parameters were measured and data obtained during a 4-day cruise from 6 to 9 August 2007, during a period of average to low discharges (150 m^3 s^{-1}) in the Watson River (Mernild and Hasholt, 2009). A Seabird SBE 19 Plus CTD (Conductivity, Temperature, and Depth) equipped with a Niskin bottle (5 L) for water sampling at 1 m depth was used for conductivity, temperature and depth profiles. The mounted optical sensors recorded photosynthetically active radiation (PAR) with a LI-COR underwater quantum sensor (Li-192). Light transmittance in the water column was measured with a Wetlabs C-Star transmissometer, mounted on the CTD with an operating wavelength of 660 nm across a path length of 25 cm. The particle beam attenuation coefficient related to particles (c_p) was derived as:

$$c_p - c_w = \ln(T_r)/r \quad (1)$$

where T_r is the transmittance, r the path length, and c_w the light attenuation coefficient in pure water (Smith and Baker, 1981). Downwelling irradiance in the interval 320–950 nm was measured with a RAMSES ACC VIS TriOS radiometer with a cable connection to a PC running the data collecting software onboard. The radiometer has a resolution of 3.3 nm, and integration time of the sensor was set to automatic and ranged from 4 to 4096 ms relative to irradiances at depths. The CTD was lowered through the water column with a descent velocity of about 0.1 m s^{-1}, and parameters were measured to a depth of about 30–35 m. Optical casts were carried out on the sunny side of the ship to avoid any shadow effects, and the CTD was lowered into the water column from a crane with a distance to the ship of about 3 m. A LI-Cor 190 PAR sensor mounted above the steering house recorded downwelling PAR with 1 min intervals during the cruise for primary production calculations. Spectral attenuation coefficients $K_d(\lambda)$ for each of the wavelengths 380, 413, 443, 489, 509, 555, 624, and 664 nm were calculated following the procedure by (Devlin et al., 2008):

$$K_d(\lambda) = -\ln((I_i(\lambda))/(I_{i-1}(\lambda)))/(z_i - z_{i-1}) \quad (2)$$

and similar for K_d(PAR):

$$K_d(PAR) = -\ln((I_i(PAR))/(I_{i-1}(PAR)))/(z_i - z_{i-1}) \quad (3)$$

where indices i–1 and i indicate neighboring vertical observations with z as distance. The statistically significant ($p < 0.001$) and strong correlation ($r^2 = 0.92$) between SPM and beam attenuation coefficient (c_p) obtained during the present cruise (Lund-Hansen et al., 2010) was applied to derive SPM concentrations at depths of K_d(PAR) and $K_d(\lambda)$. A regression line was derived based on the linear correlation analyses between SPM and $K_d(\lambda)$ for each of the eight wavelengths and for K_d(PAR) as:

$$K_d(\lambda) = K^*_{d,SPM}(\lambda)\cdot SPM + K_{d,SPM(0)}(\lambda) \quad (4)$$

$$K_d(PAR) = K^*_{d,SPM}(PAR)\cdot SPM + K_{d,SPM(0)}PAR \quad (5)$$

where $K^*_{d,SPM}(\lambda)$ and $K^*_{d,SPM}$(PAR) are the derived SPM specific attenuation coefficients from the linear regressions at wavelength (λ) and PAR. The $K_{d,SPM(0)}(\lambda)$ and $K_{d,SPM(0)}$(PAR) are the attenuation coefficients for the λ or PAR where attenuation in the water column by SPM is theoretically zero. Both $K_d(\lambda)$ and K_d(PAR) were calculated for SPM concentrations between 0.0 and 10.0 mg m^{-3} in increments of 0.5 mg m^{-3} for the 8 wavelengths and PAR. The photic depth, defined as the depth in the water column with 1% of surface light where there is a potential for photosynthesis (Kirk, 1994), was derived as $4.6/K_d(\lambda)$ and $4.6/K_d$(PAR).

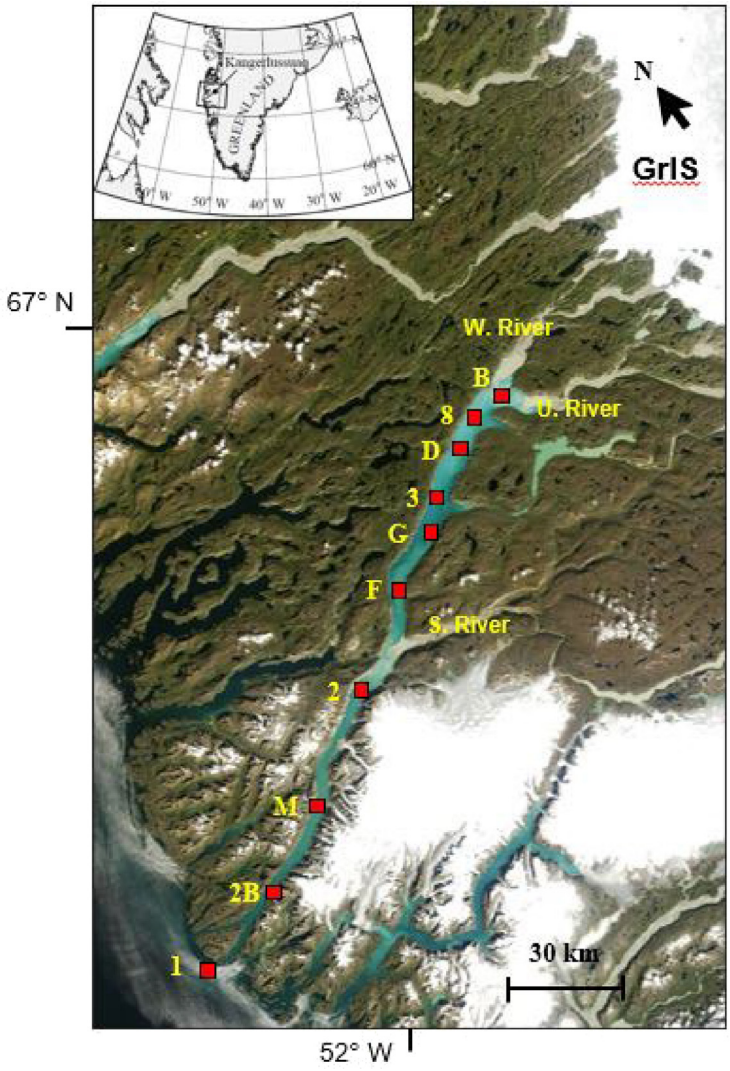

Fig. 1. MODIS image of Kangerlussuaq Fjord with sampling stations in August 2007. Greenland Ice Sheet (GrIS), Watson River (W. River), Umivit River (U. River), and Sarfartoq River (S. River).

2.3. Nutrients, Chla, and SPM

Analyses of ammonia (NH_3), nitrate (NO_3), nitrite (NO_2), silicate ($Si(OH)_4$), and phosphorus (PO_4) were conducted on filtered (Millipore Millex-GP hydrophilic PES 0.22 μm) seawater samples which were frozen and kept at −18 °C, transported to a laboratory and analyzed within 3 weeks using a SANPLUS System Scalar auto-analyzer following Grasshoff et al. (1999). Detection limits were 0.04 μM (NO_2), 0.1 μM (NO_3), 0.1 μM (NO_2), 0.2 μM ($Si(OH)_4$), and 0.2 μM for (PO_4). For Chl*a* an exact volume (0.5–1 L) of water was filtered through GF75 Advantec glass fiber filters (0.3 μm pore size), which were frozen and kept at −18 °C. Filters were transported to a laboratory, extracted in 5 mL 96% ethanol, and analyzed on a spectrophotometer (Thermo Spectronic HELIOS λ), also within 3 weeks. For SPM concentrations an exact volume (0.5–1 L) of sampled water was filtered through pre-combusted and weighed Whatman GF/F glass fiber filters (0.7 μm pore size), and filters were dried and re-weighed. Samples for nutrients, Chl*a* and nutrients were collected from 1 m depth at stations 1, 2b, 2, G, 3, and 8 with CTD, optical measurements and SPM sampling at all 10 stations (Fig. 1). SPM concentrations at depths in the water column were obtained through the beam attenuation coefficients, as described above. See Lund-Hansen et al. (2010, 2018) for more details of analyses and laboratory procedures.

2.4. Phytoplankton species

Water samples for identification of phytoplankton species were collected from 1 m depth at stations 1, 2, and 3 with a Niskin sampler, preserved with droplets of Lugol, and sent for identification by Lars Edler at WEAQ AB, Ängelholm, Sweden. Species diversity at each station was calculated as Shannon's diversity index (H), and evenness as Shannon's equitability index EH (Magurran, 1988).

2.5. Primary production

Carbon incorporation was determined using a modified ^{14}C incubation method (Steeman-Nielsen, 1952). Water samples in 8 NUNC incubation bottles (80 mL) were enriched with ^{14}C, placed in a row in a water bath at *in situ* temperature in a light gradient, where light intensity was reduced by 50% between each bottle. For more details see Lund-Hansen et al. (2018). The photosynthetic parameters P_{max} and α were derived for sampling stations 1, 2, and 3 (Fig. 1) following Jassby and Platt (1976). Primary production was calculated from the equation of (Platt et al., 1980):

$$P(z) = P_{max}(1 - \exp(-\alpha(I_o \cdot \exp(-K_d(PAR) \cdot z)/P_{max}))) \quad (6)$$

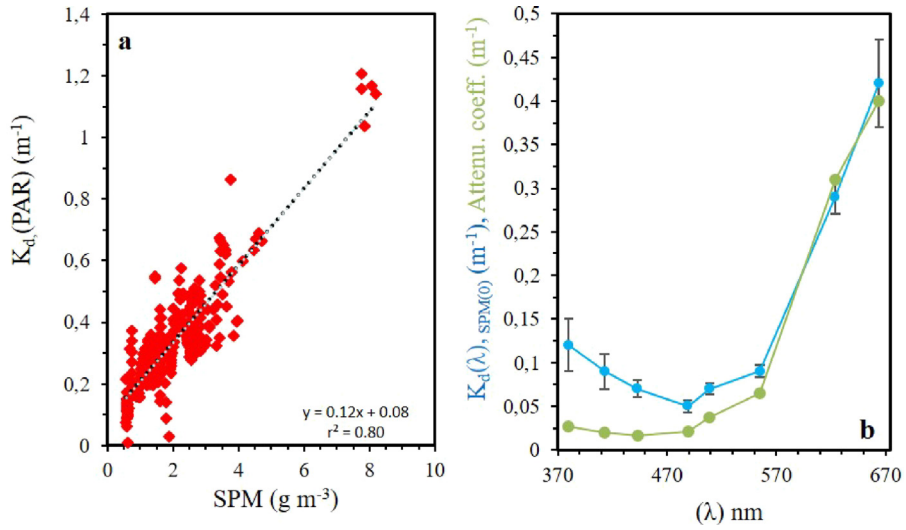

Fig. 2. A. Regression between SPM and PAR attenuation coefficients K_d(PAR) with regression equation, and B. attenuation coefficient derived from intercept with *y*-axis for the eight wavelengths in water without SPM (blue line •), compared to attenuation coefficients in pure water following Smith and Baker (1981) (green line •). . (For interpretation of the references to color in this figure legend, the reader is referred to the web version of this article.)

to quantify the relations between light attenuation, here expressed as K_d(PAR), and primary production at depths P(z), where z as depth parameter. The description of light - $I_o \cdot \exp(-K_d(PAR) \cdot z)$ - was based on measured surface PAR during the cruise and derived K_d(PAR) (3). Production per day was derived by integration down to the photic depth and summed for every hour of daylight for a day in early August.

3. Results

3.1. PAR and spectral attenuation governed by PAR

There was a strong ($r^2 = 0.80$) and statistically significant ($p < 0.001$) correlation between SPM and K_d(PAR) (Fig. 2a). The value 0.12 m^{-2} g^{-1} is the PAR SPM specific attenuation coefficient and 0.08 m^{-1} intercept, with *y*-axis as the PAR attenuation coefficient related to other optical constituents than SPM. The eight wavelengths (380, 413, 443, 489, 509, 555, 624, and 664 nm) all showed similar strong ($r^2 = 0.85 - 0.75$) and statistically significant ($p < 0.001$) correlations between SPM and $K_d(\lambda)$ (Supplementary material Tab. S1). Intercepts of the eight wavelengths and attenuation in pure water showed a difference of about 0.1 m^{-1} in the UV band at 380 nm, which gradually decreased with increasing wavelengths (Fig. 2b).

3.2. Spectral and PAR attenuation at variable SPM

Spectrally resolved photic depths (Z_0) relative to SPM concentrations showed that the 509 nm wavelength reached a maximum depth of 24 m at 1.0 g SPM m^{-3} (Fig. 3a). For concentrations >1.0 g SPM m^{-3} wavelength depth maximum changed to 555 nm. The proportions between blue and red light at 443 and 624 in the water column changed with SPM concentrations. This was demonstrated by photic depths of 11.0 m (443 nm) and 7.0 m (660 nm) at 2.0 g SPM m^{-3}, which changed to a depth of 5.0 m for both wavelengths at 5.0 g SPM m^{-3}. PAR photic depths (Z_0) decreased similarly with an increase in SPM, which showed a PAR photic depth of about 9 m for an average of 4.0 g SPM m^{-3} in August 2007 (Fig. 3b). The reduction in photic depth with increased K_d(PAR) was close to exponential, as was the case for the spectrally resolved attenuation coefficients $K_d(\lambda)$ (Fig. 3b).

3.3. Primary production and SPM

The relations between K_d(PAR) and primary production Eq. (4) were explored based on measured irradiances during hours of daylight in August and measured photosynthetic parameters: P_{max} (mg C m^{-3} h^{-1}) and α mg C m^{-3} h^{-1}(μM m^{-2} s^{-1})$^{-1}$ from marine st. 1. Results showed that primary production decreased nearly exponentially with the increase in K_d(PAR) and SPM, with a maximum primary production of 276.8 mg C m^{-2} d^{-1} at minimum K_d(PAR) of 0.1 m^{-1} (Fig. 4). SPM concentrations are shown as derived from the SPM and K_d(PAR) correlation (Fig. 2a). Production decreased significantly with an increase in K_d(PAR) at lower SPM concentrations whereas the rate of change was relatively lower at higher SPM levels.

3.4. Surface salinity, Chla, and nutrients

The transect of stations 8, 3, G, 2, 2B, and 1 with surface samples (1 m) between the inner and outer parts of the fjord (Fig. 1) showed salinities around 5 at inner stations which increased to near 30 at outer st. 1 (Fig. 5a). There was a gradual increase in Chl*a* along the transect, where lowest salinities (4.2) on the transect related to the freshwater from the Sarfartoq River at st. 2. The ($NO_2 + NO_3$) concentrations were highest near river outlets at st. 8 and 2, but with no clear distribution of NH_3 (Fig. 5b), as compared to PO_4 where concentrations showed a strong ($r^2 = 0.82$) and significant ($p < 0.01$) correlation with distance from river outlet (Fig. 5c). SiO_2 concentrations were opposite and high around 10.0 μM at inner stations (st. 8, 3, G) and at Sarfartoq river outlet (st. 2), but with low values around 2.0 μM at to outer marine stations (st. 1, 2b) (Fig. 5c).

3.5. Phytoplankton species

Only three species of phytoplankton occurred at st. 2 near the Sarfartoq river outlet though in a very high (1.37×10^6 cells L^{-1}) numbers, and dominated by *Skeletonema costatum* (Supplementary material Tab. S2). Further, Shannon's diversity index was low (0.013) at st. 2 as was Evenness (0.012), as compared to marine st. 1 with 42 species with both high (2.41) Shannon's diversity and Evenness (0.64) numbers (Fig. 6). Diversity similarity was low (14%) between st. 1 and 2 though higher (43%) between st. 2 and 3.

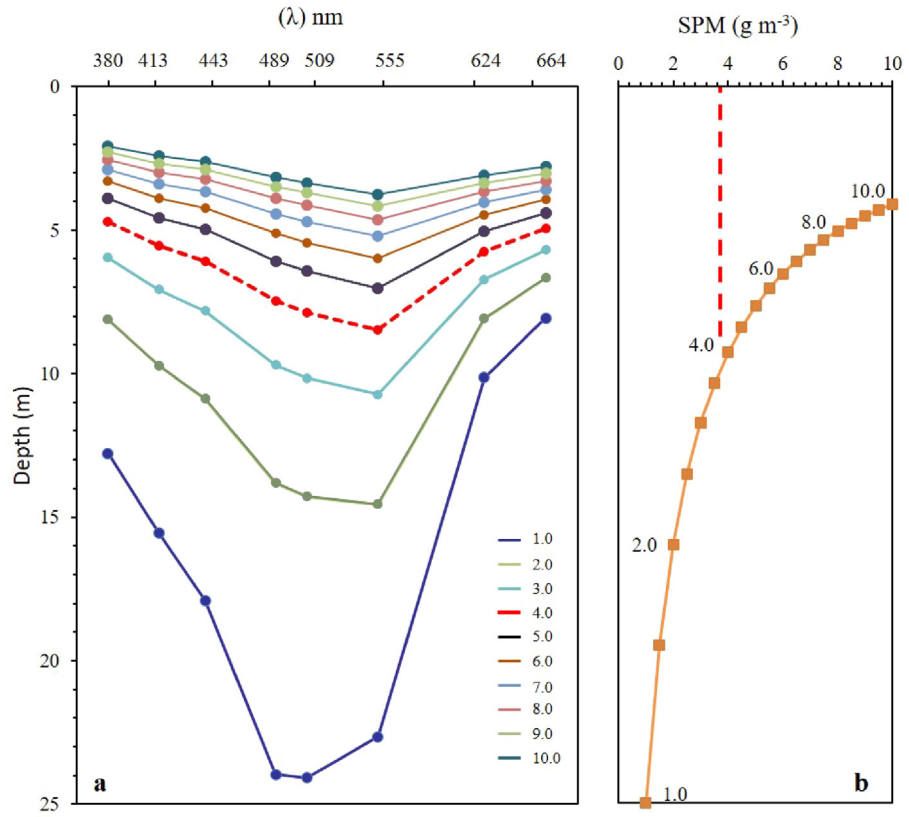

Fig. 3. A. Spectral distribution of photic depths (Z_0) relative to SPM concentrations between 1.0 and 10.0 g m^{-3} where the red hatched line is spectral photic depths for an average SPM of 4.0 g m^{-3} in August 2007, and B. PAR photic depths (Z_0) as a function of SPM concentrations where the red hatched line is PAR photic depth for an average SPM of 4.0 g m^{-3} in August 2007. . (For interpretation of the references to color in this figure legend, the reader is referred to the web version of this article.)

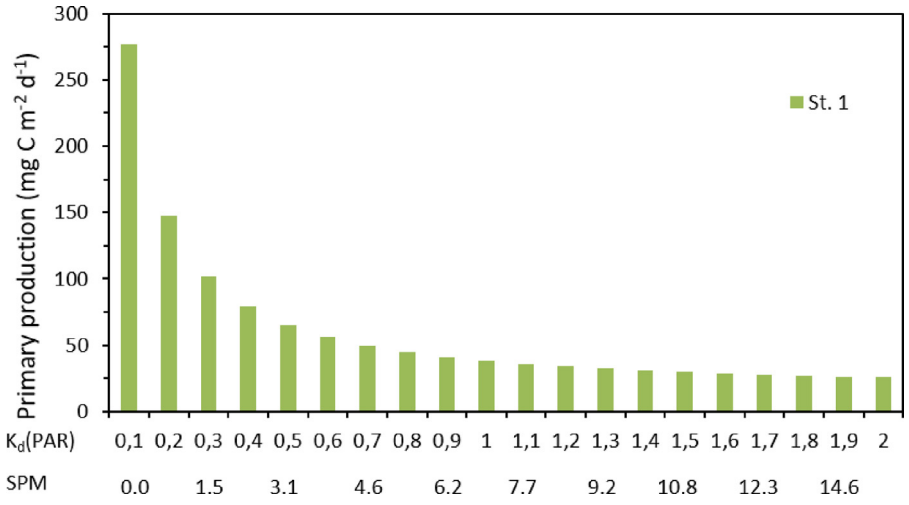

Fig. 4. Primary production at st. 1 relative to K_d(PAR) and SPM.

3.6. Plume extension and thickness

Selected profiles of SPM with depth at stations B, D, F, M, and 2B on a fjord transect (Fig. 1) showed a surface concentration of 123.3 g SPM m^{-3} at the river outlet (st. B), 4.0 g SPM m^{-3} at st. D about 50 km from river outlet, and 1.5 g SPM m^{-3}at st. 2B at 140 km from outlet (Fig. 2a). Thickness of the plume, here given as the distance between surface and a depth in the water column of relatively lower and near constant SPM concentrations, was about 10 m at river outlet st. B and about 5 m at st. D and F. At outer st. 2b SPM gradually decreased from the surface concentration of 1.5 g SPM m^{-3} to a background SPM concentration of 0.7 g SPM m^{-3} and with no clear plume. Profiles of salinity along the transect showed reduced surface salinities (2–6) at st. B, D, and F and higher (20–22) at the outer st. 2B and M (Fig. 2b). The water column down to about 30 m was affected by the discharge of meltwater given by the reduced salinities st. B, D, and F compared to st. M and 2B (Fig. 2b).

A previous study in Kangerlussuaq (McGrath et al., 2010) showed a positive correlation between Watson River discharge

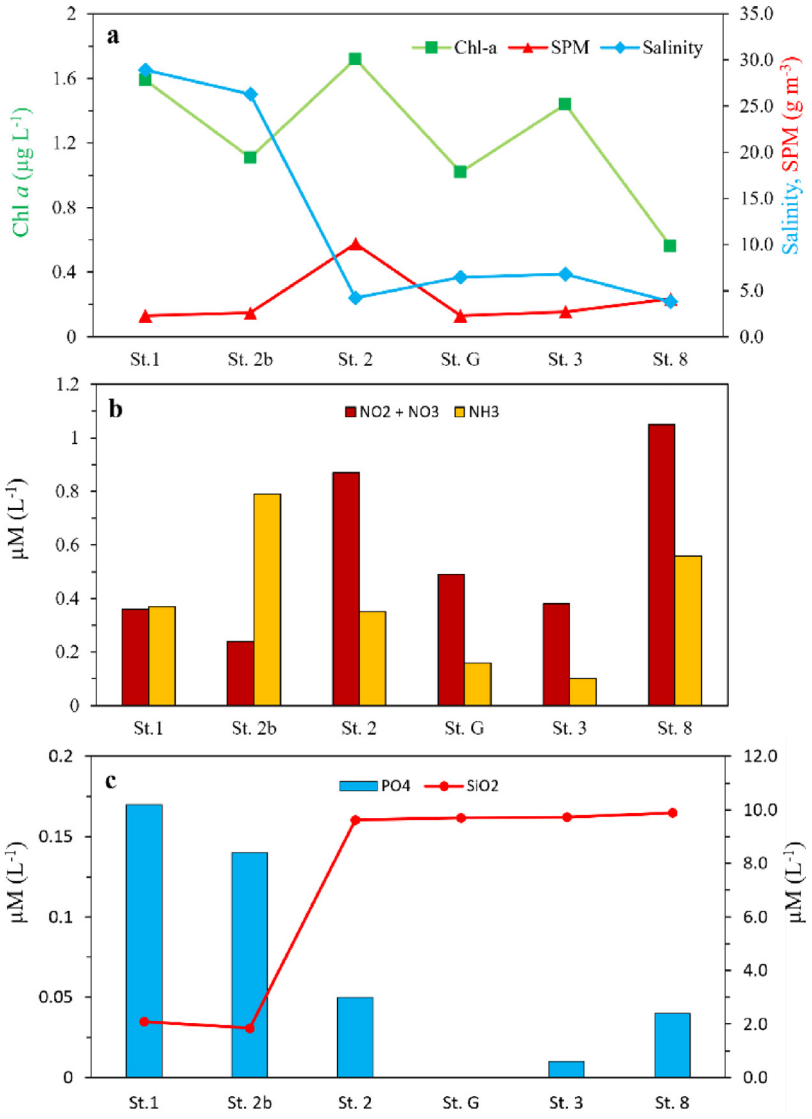

Fig. 5. A. Surface (1 m) Chl-*a*, SPM, and salinity at stations from outer marine st. 1 to near river outlet st. 8, and B. $NO_2 + NO_3$ and NH_3 concentrations at stations, and C. SiO_2 and PO_4 concentrations. Nutrient concentrations at st. 1, 2, 3 from Lund-Hansen et al. (2018). Note that present st. 2 corresponds to st. 5 and st. 3 to st. 7 in Lund-Hansen et al. (2010).

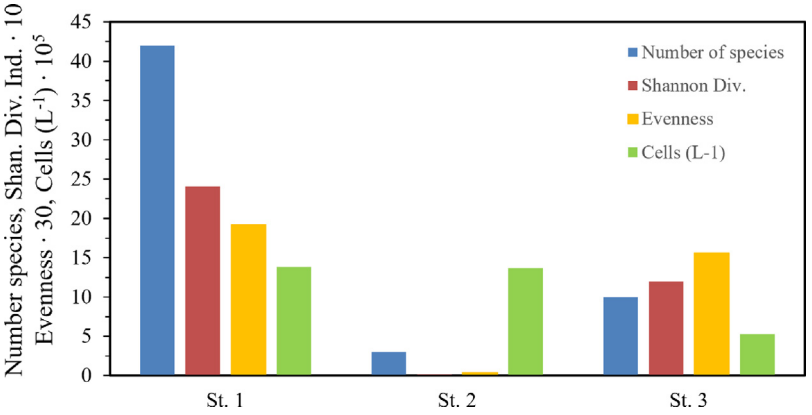

Fig. 6. Number of phytoplankton species, Shannon's diversity index, Evenness, and cells L^{-1} at st. 1, 2, and 3 at 1 m depth. Note that diversity index was multiplied by 10, and Evenness by 30.

and plume length, which gave a 20% coverage of the fjord at an early August discharge of 250 m^3 s^{-1} (Hasholt et al., 2012). Discharges and sediment load from the Sarfartoq River are unknown, but concentrations reached 10 g SPM m^{-3} at the st. 2 Sarfartoq River outlet, and decreased gradually towards st. 2b (Figs. 1 and 7). This establishes a second plume in Kangerlussuaq, which was

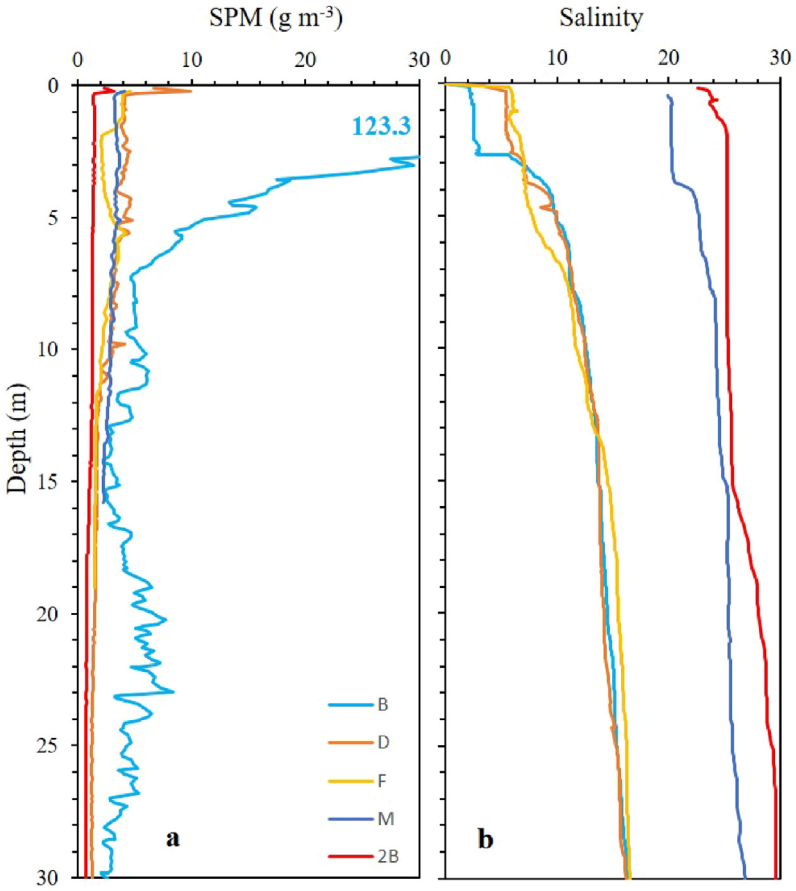

Fig. 7. Selected profiles of SPM concentrations (a), and salinity (b) at st. 2B, M, F, D, and B where the number of 123.3 is the SPM concentration in the surface layer at 1 m depth. Vertical resolution of SPM signal is 0.1 m.

about 50 km long and covered about 160 km^2 equal to 33% of the total area. This indicates that the meltwater plume influenced about 50% of the surface area in Kangerlussuaq in August 2007.

4. Discussion

4.1. PAR and spectral attenuation

The strong ($r^2 = 0.80$) and significant ($p < 0.001$) linear correlation between SPM and K_d(PAR) demonstrated that PAR attenuation in Kangerlussuaq was closely governed by the SPM. This was further emphasized by the low (0.08 m^{-1}) PAR attenuation coefficient in the water column with no attenuation caused by SPM, but supposedly CDOM in the blue and UV part of the spectrum (Kirk, 1994). This is supported by the observation that the difference between attenuation in pure water (Smith and Baker, 1981) and attenuation observed was 0.1 m^{-1} at 360 nm, and that the difference decreased with increasing wavelengths. Photic depth (Z_0), defined as the depth in the water column to which primary production can occur and taken as the depth where there is 1% left of the surface 100% irradiance (Kirk, 1994), was also negatively correlated with SPM concentrations. For instance, Z_0 for PAR was about 9 m at current average SPM concentrations of 4.0 g SPM m^{-3} but was more than halved to about 4 m of depth at SPM of 10.0 g SPM m^{-3}. The spectral composition of light in the water column was strongly influenced by the SPM concentrations where the photic depth of blue light (440 nm) was 18 m and that for red light (624 nm) 10 m at 1.0 g SPM m^{-3}. The photic depth was about 5 m for both wavelengths at the average SPM concentration of 4.0 g SPM m^{-3}. This demonstrates that the attenuation of blue light in the water column increased with increased SPM concentrations. The significant reduction in the depth of blue light with increased SPM might affect photosynthesis in the water column, as Chl*a*, the main light-absorbing pigment, has two absorption peaks at 440 and 660 nm with an optimal absorption ratio of 1.3 (Johnsen, 2014). The observed increase in light attenuation in the UV-A and violet–blue parts of the spectrum at increasing SPM concentrations indicates that high turbid waters has a potential to protect the phytoplankton from the damaging effects of UV radiation, as also noted by Retamal et al. (2007) and Fritz et al. (2008). The major effects of increased SPM concentrations were the strong increase in K_d(PAR) and $K_d(\lambda)$, significant reductions in photic depths, and changes in spectral composition of the light in the water column.

4.2. Primary production and light limitation

Models or relations describing primary production in time and space are complex based on photosynthetic parameters, light, grazing by copepods, nutrient concentrations, self-shadowing, sinking of particles, and Chl*a* among other factors (Mattei et al., 2021). Here we applied a very simple approach and calculated primary production as a function of only light in the water column expressed through K_d(PAR), and based on the measured photosynthetic parameters at marine st. 1. The two approaches are not directly comparable, as the present is a description at one point in space for a daily cycle where only particulate matter concentrations, and thus K_d(PAR) varied. Cloern (1987) showed, in support of the simple approach, that a basic equation for

primary production based on Chl*a*, light and photic depths, could explain a very high percentage of the observed spatial variation in primary production in San Francisco Bay. Our results showed here that primary production relative to K_d(PAR) exposed a near exponential decrease in primary production with the gradual increase in K_d(PAR). With light as the major limiting factor in photosynthesis it is, however, strongly assumed that obtained results aligns with actual primary production being based on both based on measured K_d(PAR) and photosynthetic parameters. Our results imply, however, that once light conditions in a fjord or estuary are already turbid and limited with related reduced primary production, as in many estuaries and fjords (Gameiro et al., 2011), production will not be lowered significantly at increased SPM and higher K_d(PAR) attenuations. This calls for further research to verify the findings, where we applied a very simple, but generally accepted equation for calculating primary production.

4.3. Nutrients and Chla

Nutrients were all low (<0.5 μM), except for SiO_2 with concentrations of 10 μM at inner st. 8, 3, and 2, but down to 2.0 μM at the outer marine st. 1. The differences in SiO_2 concentrations and the clear gradient reflects the meltwater as a significant source of SiO_2 supplied to the fjord, related to weathering and denudation processes in the catchment area. The statement is supported by the fact that the SiO_2 transport to Kangerlussuaq amounts to an annual average load of 3659 tons of SiO_2 via the Watson River (Yde et al., 2014). The solute transport of SiO_2 also explains the increased SiO_2 levels around 10.0 μM at st. 2, which is dominated by meltwater from the Sarfartoq River. Annual average (2007–2010) solute transport of NO_3 with the meltwater to Kangerlussuaq reached 531 tons y^{-1} with an average NO_3 concentration of 2–3 μM, measured in the meltwater at the Watson River gauging station (Yde et al., 2014). The PO_4 concentrations were not measured in the Watson River (Yde et al., 2014), but low concentrations at river outlets at st. 2 and 8, strongly indicate that solute transport of PO_4 with the meltwater is low. The statement is supported by other observations in Greenland (Hawkings et al., 2015), as PO_4 and other forms of phosphate are adsorbed to sediment particles in the meltwater and not measured in the solute (Bagshaw et al., 2016). The positive correlation between distance and PO_4 concentrations indicated that marine waters have higher PO_4 concentrations compared to the meltwater influenced part of the fjord. Surplus of meltwater with nutrients is discharged out of Kangerlussuaq, but the ratio between how much of the NO_3 is taken up primary production in the fjord and how much is transported out of the fjord unknown. This might also depend on season of the year and the volume of meltwater discharged into Kangerlussuaq. It has been pointed out that nutrients in glacial meltwater can be significant nutrient sources regarding primary production in the related shelf areas (Oliver et al., 2018).

4.4. Phytoplankton

The significant differences in the number of phytoplankton species, with the highest (42) at the marine st. 1 and the lowest (3) at st. 2, were paralleled in the Evenness and Diversity indexes, whereas the number of cells L^{-1} were very similar at st. 1 (13.8×10^5) and st. 2 (13.7×10^5). The diatom *Skeletonema costatum* accounted for >99% of the community at st. 2, 65% at st. 3, and 12% at st. 1. In both limnic (Laird et al., 2021) and marine (Muylaert et al., 1999; Liu et al., 2018) communities, the number of diatom species often decreases with increased turbidity, which is in line with our observations of the 99% dominance of *Skeletonema costatum* at st. 2 in the meltwater plume from Sarfartog River. *Skeletonema costatum* is a euryhaline species that thrives, in terms of growths rates, in a wide range of salinities down to 2–3 (Balzano et al., 2011). The number of *Skeletonema costatum* cells appeared, on the other hand, not to be affected by differences in surface water PAR, shown by a comparison of an estuarine section with dredging and increased turbidity around 100 μM m^{-2} s^{-1} and an un-dredged section with 800 μM m^{-2} s^{-1} (Nayar et al., 2005). The SiO_2 was in surplus at both st. 2 and 3, being an important component in the frustules of the diatom (Bondoc et al., 2016), but it remains unclear why only *Skeletonema costatum* and not any other diatom species occurred in such high numbers there (Supplementary material Tab. S2).

4.5. Discharges, particulate matter, and meltwater plume

The positive correlation between increased air temperatures and increased meltwater discharges from GrIS has been demonstrated in several studies (Hanna et al., 2008; Broeke et al., 2017; Young et al., 2022). The meltwater discharges in the Watson River at Kangerlussuaq are likewise related to air temperatures, but also snow and albedo conditions in the Watson River catchment area on the GrIS (As et al., 2012), and which differ between years (Hasholt et al., 2012). McGrath et al. (2010) showed that the length of meltwater plume in Kangerlussuaq was positively correlated with an average of 4 days discharge, and that plume coverage was strongly correlated with plume length. Our estimates based on SPM profiles indicated that about 50% of the surface area in Kangerlussuaq was influenced by the meltwater plume in August 2007, at even average discharges. Plume thickness was about 10 m in August 2007 where SPM concentrations gradually decreased with depth, and clearly with distance. The tidal range is up to 3 m, which generates a flow of water that can affect position and location of the plume, but there are currently no data available on current speeds from the fjord. The climate at Kangerlussuaq is inland climate, with low wind speeds, whereby the effects of wind driven currents and displacements of the plume are presumably minimal.

4.6. Kangerlussuaq in comparison

The K_d(PAR) reached an average of 0.56 m^{-1} in Kangerlussuaq as compared to an average K_d(PAR) of 0.4 m^{-1} in Young Sound, a land-terminating glacial fjord in north-east Greenland, and 0.3 m^{-1} in the Godthåbs Fjord in south-west Greenland, with both land- and water-terminating glaciers (Murray et al., 2013). With low CDOM absorptions coefficients and Chl*a* concentrations, this study concluded that SPM was the governing parameter regarding light attenuation in these two fjords (op. cit.). Light attenuation in Kangerlussuaq was similarly governed by SPM, with comparable low CDOM and Chl*a* concentrations as in Young sound and Godthåbs Fjord (Lund-Hansen et al., 2010; Murray et al., 2013). The relatively higher K_d(PAR) in Kangerlussuaq might be related to fine grain sizes here as discussed by Lund-Hansen et al. (2010), as finer grain sizes attenuate the light relatively more efficiently (Bright et al., 2020). In comparison, the present nutrient concentrations were very similar to those measured in Young Sound with $NO_3 + NO_2 < 0.5$ μM, PO_4 of 0.2–0.3 μM, and where SiO_2 was about 10 times lower in Young Sound (<1.0 μM) (Rysgaard et al., 1999). Average Kangerlussuaq Fjord Chl*a* reached 1.2 mg Chl*a* m^{-3}, about two times higher compared to surface values of <0.5 mg Chl *a* m^{-3} in Young Sound in August (Rysgaard et al., 1999). The primary production rate of 247 mg C m^{-2} d^{-1} at st. 1 in Kangerlussuaq (Lund-Hansen et al., 2018) compares to the August production of 200 mg C m^{-2} d^{-1} in Disko Bay north of Kangerlussuaq (Levinsen and Nielsen, 2002). Rates are also comparable to the 50–200 mg C m^{-2} d^{-1} measured in Young Sound (Holding et al., 2019). The similarity between

K_d(PAR) levels, nutrient and Chl-*a* concentrations, and primary production rates in Kangerlussuaq and Young Sound, emphasizes the importance of being a land-terminated glacial fjord rather than variations related to latitudes, spatial scales, hydrodynamics, or morphology.

5. Conclusions

1. Light attenuation in Kangerlussuaq, both PAR and spectrally, were strongly governed by SPM concentrations, as demonstrated by a significant and positive correlations between SPM and K_d(PAR) as for the wavelengths 380, 413, 443, 489, 509, 555, 624, and 664 nm. Spectral composition of light in the water column changed with SPM concentrations.
2. Photic depths in the water column were strongly governed by SPM concentrations, and both for PAR and the wavelengths 380, 413, 443, 489, 509, 555, 624, and 664 nm.
3. The relation between SPM in terms of K_d(PAR) and primary production showed a strong dependency, where primary production decreased nearly exponentially with the increase in K_d(PAR). The variation in primary production is accordingly most pronounced at low K_d(PAR). Once K_d(PAR) or SPM reach above a certain level of about $K_d(PAR) = 0.5\ m^{-1}$ or of 3.1 g SPM m^{-3} changes in primary production were less pronounced.
4. The low concentrations of $(NO_3 + NO_2)$ and NH_3 and variations in concentrations were not related to any meltwater characteristics as distances or particulate matter concentrations, whereas SiO_2 concentrations clearly decreased with distance from meltwater source, whereas PO_4 concentrations in contrast increased.
5. The number of phytoplankton species was clearly much lower in the meltwater-influenced water column and accordingly also the diversity. The number of phytoplankton cells was similar at all stations and was strongly dominated by *Skeletonema costatum* in the meltwater plume.
6. We estimate that about 50% of the surface area of Kangerlussuaq was influenced by the meltwater plume of varying concentrations with a varying thickness between 5 and 10 m and deepest near meltwater outlet.

CRediT authorship contribution statement

Lars Chresten Lund-Hansen: Writing – original draft, Formal analysis, Visualization, Conceptualization, Project administration. **Ingela Dahllöf:** Writing – original draft, Formal analysis, Data curation. **Morten Holtegaard Nielsen:** Writing – original draft, Formal analysis, Project administration.

Declaration of competing interest

The authors declare that they have no known competing financial interests or personal relationships that could have influenced the work reported in this paper.

Data availability

Data will be made available on request.

Acknowledgments

The initial project was supported by an International Polar Year grant for the Commission of Scientific Research in Greenland (KVUG), and further developed in the frame of the project FACE-IT (The Future of Arctic Coastal Systems - Identifying Transitions in Fjord Systems and Adjacent Coastal Areas). FACE-IT has received funding from European Union's Horizon 2020 research and innovation program under grant number agreement No 869154. Captain and crew onboard "Navarana" are thanked for all their efforts during the cruise in Kangerlussuaq.

Appendix A. Supplementary data

Supplementary material related to this article can be found online at https://doi.org/10.1016/j.rsma.2023.103054.

References

Aksnes, D.L., Nejstgaard, J., Sædberg, E., Sørnes, T., 2004. Optical control of fish and zooplankton populations. Limnol. Oceanogr. 49, 233–238. http://dx.doi.org/10.4319/lo.2004.49.1.0233.

Arndt, K.E., Dutz, J., Jónasdottir, S.H., J.-Madsen, S., Mortensen, J., Møller, E.F., Nielsen, T.G., 2011. Effects of suspended sediments on copepods feeding in a glacial influenced sub-Arctic fjord. J. Plankton Res. 33, 1526–1537. http://dx.doi.org/10.1093/plankt/fbr054.

Arrigo, K.R., Dijken, G.L., Castelao, R.M., Luo, H., Rennermalm, Å.K., Tedesco, M., Mote, T.L., Oliver, H., Yager, P.L., 2017. Melting glaciers stimulate large summer phytoplankton blooms in southwest Greenland waters. Geophys. Res. Lett. 44, 6278–6285. http://dx.doi.org/10.1002/2017GL073583.

As, D., Hubbard, A.L., Hasholt, B., Mikkelsen, A.B., Broeke, M.R., Fausto, R.S., 2012. Large surface meltwater discharge from the Kangerlussuaq sector of the Greenland ice sheet during the record-warm year 2010 explained by detailed energy balance observations. Cryosphere 6, 199–209. http://dx.doi.org/10.5194/tc-6-199-2012.

Bagshaw, E.A., Beaton, A., Wadham, J.L., Mowlem, M., Hawkings, J.R., Tranter, M., 2016. Chemical sensors for in situ data collection in the cryosphere. Trends Anal. Chem. 82, 348–357. http://dx.doi.org/10.1016/j.trac.2016.06.016.

Balzano, S., Sarno, D., Wiebe, H., Kooistra, F., 2011. Effects of salinity on the growth rate and morphology of ten Skeletonema strains. J. Plankton Res. 33, 937–945. http://dx.doi.org/10.1093/plankt/fbq150.

Bondoc, K.G.V., Heuschele, J., Gillard, J., Vyverman, W., Pohnert, G., 2016. Selective silicate-directed motility in diatoms. Nat. Commun. 7, 10540. http://dx.doi.org/10.1038/ncomms10540.

Box, J., Colgan, W.T., Christensen, T.R., Schmidt, N.M., Lund, M., Parmentier, F.-J., Brown, R., Bhatt, U., Eusjirchen, E.S., Romanovsky, V.E., Walsh, J.E., Overland, J.E., Wang, M., Corell, R.W., Meier, W.-N., Wouters, B., Mernild, S., Mård, J., Pawlak, J., Olsen, M.S., 2019. Key indicators of Arctic climate change. Environ. Res. Lett. 14, 045010. http://dx.doi.org/10.1088/1748-9326/aafc1b.

Bright, C., Mager, S., Horton, S., 2020. Response of nephelometric turbidity to hydrodynamic particle size of fine suspended sediment. Int. J. Sedim. Res. 35, 444–454. http://dx.doi.org/10.1016/j.ijsrc.2020.03.006.

Broeke, M., Box, J., Fettweis, X., Hanna, E., Noël, B., Tedesco, M., As, D., Berg, W.J., Kampenhout, L., 2017. Greenland ice sheet surface mass loss: Recent developments in observation and modeling. Curr. Clim. Change Rep. 3, 345–356. http://dx.doi.org/10.1007/s40641-017-0084-8.

Cantoni, C., Hopwood, M.J., Clarke, J.S., Chiggiato, J., Achterberg, E.P., Cozzi, S., 2020. Glacial drivers of marine biogeochemistry indicate a future shift to more corrosive conditions in an Arctic fjord. J. Geophys. Res. Biogeosci. 125, e2020JG005633. http://dx.doi.org/10.1029/2020JG005633.

Cloern, J.E., 1987. Turbidity as a control on phytoplankton biomass and productivity in estuaries. Cont. Shelf Res. 7, 1367–1381. http://dx.doi.org/10.1016/0278-4343(87)90042-2.

Cook, A.J., Copland, L., Noël, B.P.Y., Stokes, C.R., Bentley, M.J., Sharp, M.J., Bingham, R.G., Broeke, M.R., 2019. Atmospheric forcing of rapid marine-terminating glacier retreat in the Canadian Arctic Archipelago. Sci. Adv. 5, http://dx.doi.org/10.1126/sciadv.aau8507.

Crumley, R.L., Hill, D.F., Beamer, J.P., Holzenthal, E.R., 2017. Seasonal components of freshwater runoff in Glacier Bay, Alaska: diverse spatial patterns and temporal change. Cryosphere 13, 1597–1619, doi: TC - Seasonal components of freshwater runoff in Glacier Bay, Alaska....

Davies, B.J., Glasser, N.F., 2017. Accelerating shrinkage of patagonian glaciers from the Little Ice Age (∼AD 1870) to 2011. J. Glaciol. 58, 1063–1084. http://dx.doi.org/10.3189/2012JoG12J026.

Devlin, M.J., Barry, J., Mills, D.K., Gowen, R.J., Foden, J., Sivyer, D., Tett, P., 2008. Relationships between suspended particulate matter light attenuation and Secchi depth in UK marine waters. Estuar. Coast. Shelf Sci. 79, 429–439. http://dx.doi.org/10.1016/j.ecss.2008.04.024.

Eaves, S.R., Anderson, B.M., Mackintosh, A.N., 2017. Glacier-based climate reconstructions for the last glacial-interglacial transition: Arthur's Pass, New Zealand (43° S). J. Quarter. Sci. 32, 877–887. http://dx.doi.org/10.1002/jqs.2904.

Falkowski, P.G., Raven, J.A., 2007. Aquatic Photosynthesis, second ed. Princeton University Press, p. 488.

Fritz, J.J., Neale, P.J., Davis, R.F., Peloquin, J.A., 2008. Response of antarctic phytoplankton to solar UVR exposure: inhibition and recovery of photosynthesis in coastal and pelagic assemblages. Mar. Ecol. Prog. Ser. 365, 1–16. http://dx.doi.org/10.3354/meps07610.

Gameiro, C., Zwolinski, J., Brotas, V., 2011. Light control on phytoplankton production in a shallow and turbid estuarine system. Hydrobiologia 669, 249–263. http://dx.doi.org/10.1007/s10750-011-0695-3.

Gillard, L.C., Hu, X., Myers, P.G., Bamber, J.L., 2016. Meltwater pathways from marine terminating glaciers of the Greenland ice sheet. Geophys. Res. Lett. 43, 10873–10882. http://dx.doi.org/10.1002/2016GL070969.

Grasshoff, K., Erhardt, M., Kremlin, K. (Eds.), 1999. Methods of Seawater Analysis. Wiley, London, p. 632.

Halbach, L., Vihtakari, V., Duarte, P., Everett, A., Granskog, M.A., Hop, H., Kauko, H.M., Kristiansen, S., Myhre, P.I., Pavlov, A.K., Pramanik, A., Tatarek, A., Torsvik, T., Wiktor, J.M., Wold, A., Wulff, A., Steen, Assmy, P., 2019. Tidewater Glaciers and bedrock characteristics control the phytoplankton growth environment in a fjord in the Arctic. Front. Mar. Sci. 6, 254. http://dx.doi.org/10.3389/fmars.2019.00254.

Hanna, E.P., Huybrecths, P., Steffen, K., Cappelen, R., Huff, R., Shuman, C., Tristram, I.F., Wise, S., Griffiths, M., 2008. Increased runoff from meltwater from the Greenland ice sheet: A response to global warming. J. Clim. 15, 331–341. http://dx.doi.org/10.1175/2007JCLI1964.I.

Hasholt, B., Mikkelsen, A., Nielsen, M.H., Larsen, M.A.D.L., 2012. Observations of runoff and sediment and dissolved loads from the Greenland ice sheet at Kangerlussuaq, West Greenland, 2007 to 2010. Z. Geomorphol. http://dx.doi.org/10.1127/0372-8854/2012/S-00121, Suppl. Issue.

Hawkings, J.R., Wadham, J.L., Tranter, M., Lawson, E., Sole, A., Cowton, T., Tedstone, A.J., Bartholomew, I., Niewnow, P., Chandler, D., Telling, J., 2015. The effect of warming climate on nutrient and solute export from the Greenland Ice Sheet. Geochim. Pers. Lett. 1, 94–104. http://dx.doi.org/10.7185/geochemlet.1510.

Holding, J.M., Markager, S., J.-Pedersen, T., Paulsen, M.L., Møller, E.F., Meire, L., Sejr, M., 2019. Seasonal and spatial patterns of primary production in a high-latitude fjord affected by Greenland Ice Sheet run-off. Biogeosciences 16, 3777–3792. http://dx.doi.org/10.5194/bg-16-3777-2019.

Hopwood, M.J., Carroll, D., Dunse, T., Hodson, A., Holding, J.M., Iriarte, J.L., Ribeiro, S., Achterberg, E.P., Cantoni, C., Carlson, D., Chierici, M., Clarke, J.S., Cozzi, S., Fransson, A., Juul-Pedersen, T., Winding, M., Meire, L., 2020. Review article: How does glacier discharge affect marine biogeochemistry and primary production in the Arctic? Cryosphere 14, 1347–1383. http://dx.doi.org/10.5194/tc-14-1347-2020.

Hopwood, M.J., Connelly, D.P., Arendt, K.E., Juul-Pedersen, T., Stinchcombe, M.C., Meire, L., Esposito, M., Krishna, R., 2016. Seasonal changes in Fe along a glaciated Greenlandic fjord. Front. Earth Sci. 4, 15. http://dx.doi.org/10.3389/feart.2015.00015.

Huang, J., Zhang, X., Zhang, Q., Lin, Y., Hao, M., Luo, Y., Zhao, Z., Chen, X., wang, L., Nie, S., Yin, Y., Xu, Y., Zhang, J., 2017. Recently amplified arctic warming has contributed to a continual global warming trend. Nat. Clim. Chang. 7, 875–879. http://dx.doi.org/10.1038/s41558-017-0009-5.

Hudson, B., Overeem, I., McGrath, D., Syvitski, J.P.M., Mikkelsen, A.B., Hasholt, B., 2014. MODIS observed increase in duration and spatial extent of sediment plumes in Greenland fjords. Cryosphere 8, 1161–1176. http://dx.doi.org/10.5194/tc-8-1161-2014.

Jassby, A.D., Platt, T., 1976. Mathematical formulation of the relationship between photosynthesis and light for phytoplankton. Limnol. Oceanogr. 21, 540–547. http://dx.doi.org/10.4319/lo.1976.21.4.0540.

Johnsen, S., 2014. Hide and seek in the open sea: Pelagic camouflage and visual countermeasures. Annu. Rev. Mar. Scí. 6, 369–392. http://dx.doi.org/10.1146/annurev-marine-010213-135018.

Kienholz, C., Herreid, S., Rich, J.L., Arendt, A.A., Hock, R., Burgess, E.W., 2015. Derivation and analysis of a complete modern-data glacier inventory for Alaska and northwest Canada. J. Glaciol. 61, 403–420. http://dx.doi.org/10.3189/2015JoG14J230.

Kirk, J.T.O., 1994. Light and Photosynthesis in the Aquatic Ecosystems. Cambridge University Press, p. 509.

Laird, K.R., Barouillet, C., Cumming, B.F., Perrin, C.J., Selbie, D.T., 2021. Influence of glacial turbidity and climate on diatom communities in two fjord lakes (British Columbia, Canada). Aquat. Sci. 82, 13. http://dx.doi.org/10.1007/s00027-020-00767-3.

Levinsen, H., Nielsen, T.G., 2002. The trophic role of marine pelagic ciliates and heterotrophic dinoflagellates in arctic and temperate coastal ecosystems: A cross-latitude comparison. Limnol. Oceanogr. 47, 427–439. http://dx.doi.org/10.4319/lo.2002.47.2.0427.

Liu, B., Swart, H.E., Jonge, V.N., 2018. Phytoplankton bloom dynamics in turbid, well-mixed estuaries: A model study. Estuar. Coast. Shelf Sci. 211, 137–151. http://dx.doi.org/10.1016/j.ecss.2018.01.010.

Lund-Hansen, L.C., Andersen, T.J., Nielsen, M.H., Pejrup, M., 2010. Suspended matter, Chl-a, CDOM, grain sizes, and optical properties in the Arctic fjord-type estuary, Kangerlussuaq, West Greenland during summer. Estuar. Coast. 33, 1442–1451. http://dx.doi.org/10.1007/s12237-010-9300-7.

Lund-Hansen, L.C., Hawes, I., Nielsen, M.H., Dahllöf, Sorrell, B.K., 2018. Summer meltwater and spring sea ice primary production, light climate and nutrients in an Arctic estuary, Kangerlussuaq, west Greenland. Arct. Antarct. Alp. Res. 50, 1. http://dx.doi.org/10.1080/15230430.2017.1414468.

Lund-Hansen, L.C., Hawes, I., Sorrel, B.K., Nielsen, M.H., 2014. Removal of snow cover inhibits spring growth of Arctic ice algae through physiological and behavioral effects. Pol. Biol. 37, 471–481. http://dx.doi.org/10.1007/s00300-013-1444-z.

Magurran, A.E., 1988. Ecological Diversity and its Measurements. Chapman & Hall, UK, p. 180. http://dx.doi.org/10.1007/978-94-015-7358-0.

Mattei, F., Buonocore, E., Franzese, P.P., Scardi, M., 2021. Global assessment of marine phytoplankton primary production: Integrating machine learning and environmental accounting models. Ecol. Model. 451, 109578. http://dx.doi.org/10.1016/j.ecolmodel.2021.109578.

Mayer, C., Schuler, T., 2005. Breaching of an ice dam at Qorlortossup tasia, south Greenland. Ann. Glaciol. 42, 297–302. http://dx.doi.org/10.3189/172756405781812989.

McGrath, D., Steffen, K., Overeem, I., Mernild, S.H., Hasholt, B., Broeke, M., 2010. Sediment plumes as a proxy for local ice-sheet runoff in Kangerlussuaq Fjord, West Greenland. J. Glaciol. 56, 813–821. http://dx.doi.org/10.3189/002214310794457227.

Meire, L.L., Mortensen, J., Meire, P., J.-Pedersen, T., Sejr, M., Rysgaard, S., Huybrecths, F.J., 2017. Marine-terminating glaciers sustain high productivity in Greenland fjords. Glob. Chang. Biol. 23, 5344–5357. http://dx.doi.org/10.1111/gcb.13801.

Mernild, S.H., Hasholt, B., 2009. Observed runoff, jökulhlaups and suspended sediment load from the Greenland ice sheet at Kangerlussuaq, West Greenland, 2007 and 2008. J. Glaciol. 55, 855–858. http://dx.doi.org/10.3189/002214309790152465.

Möller, M., Obleitner, F., Reijmer, C.H., Pohjola, V.A., Glowacki, P., Kohler, J., 2016. Adjustment of regional climate model output for modeling the climatic mass balance of all glaciers on svalbard. Atmosph. 121, 5411–5429. http://dx.doi.org/10.1002/2015JD024380.

Murray, C., Markager, S., Stedmon, C.A., Juul-Pedersen, T., Sejr, M.K., Bruhn, A., 2013. The influence of glacial melt water on bio-optical properties in two contrasting Greenlandic fjords. Estuar. Coast. Shelf Sci. 163, 72–83. http://dx.doi.org/10.1016/j.ecss.2015.05.041.

Muylaert, K., Tackx, M., Vyverman, W., 1999. Phytoplankton growth rates in the freshwater tidal reaches of the Schelde estuary (Belgium) estimated using a simple light-limited primary production model. Hydrobiologia 540, 127–140. http://dx.doi.org/10.1007/s10750-004-7128-5.

Nayar, S., Goh, B.P.L., Chou, L.M., 2005. Dynamics in the seize structure of Skeletonema costatum (Greville) Cleve under conditions of reduced photosynthetically available radiation in a dredged tropical estuary. J. Exp. Mar. Biol. Ecol. 318, 163–182. http://dx.doi.org/10.1016/j.jembe.2004.12.013.

Nielsen, M.H., E.-Hansen, D.R., Knudsen, K.L., 2010. Water masses in Kangerlussuaq, a large fjord in West Greenland: the processes of formation and the associated foraminiferal fauna. Pol. Res. 29, 159–175. http://dx.doi.org/10.3402/polar.v29i2.6063.

Nishizawa, B., Kanna, N., Abe, Y., Ohashi, Y., Sakakibara, D., Asaji, I., Sugiyama, S., Yamaguchi, A., Watanuki, Y., 2020. Contrasting assemblages of seabirds in the subglacial meltwater plume and oceanic water of Bowdoin Fjord, northwestern Greenland. ICES J. Mar. Sci. 77, 711–720. http://dx.doi.org/10.1093/icesjms/fsz213.

Oliver, H., Luo, H., Castelao, R.M., van Dijken, G.L., Mattingly, K.S., Rosen, J.J., 2018. Exploring the potential impact of Greenland meltwater on stratification, photosynthetically active radiation, and primary production in the Labrador Sea. J. Geophys. Res. Oceans 123, 2570–2591. http://dx.doi.org/10.1002/2018JC013802.

Overeem, I., Hudson, B.D., Syvitski, J.P.M., Mikkelsen, A.B., Hasholt, B., Broeke, M.R., Noël, B.P.Y., Morlighem, M., 2017. Substantial export of suspended sediment to the global oceans from glacial erosion in Greenland. Nat. Geosci. 10, http://dx.doi.org/10.1038/NGEO3046.

Platt, T., Gallegos, C.L., Harrison, W.G., 1980. Photoinhibition of photosynthesis in natural assemblages in marine phytoplankton. J. Mar. Res. 38, 687–701.

Retamal, L., Vincent, W.F., Martineau, C., Osburn, C.L., 2007. Comparison of the optical properties of dissolved organic matter in two river-influenced coastal regions of the Canadian Arctic. Estuar. Coast. Shelf Sci. 72, 261–272. http://dx.doi.org/10.1016/j.ecss.2006.10.022.

Rosa, K.M., Perondi, C., Veettil, B.K., Auger, J.D., Simones, J.C., 2020. Contrasting responses of land-terminating glaciers to recent climate variations in King George Island. Antarct. Sci. 32, 398–407. http://dx.doi.org/10.1017/S0954102020000279.

Rysgaard, S., Nielsen, T.G., Hansen, B.W., 1999. Seasonal variation in nutrients, pelagic primary production and grazing in a high-Arctic coastal marine ecosystem, Young Sound, Northeast Greenland. Mar. Ecol. Prog. Ser. 179, 13–25. http://dx.doi.org/10.3354/meps/179013.

Smith, R.C., Baker, K.S., 1981. Optical properties of the clearest natural waters (200-800 nm). Appl. Opt. 37, 2216–2227. http://dx.doi.org/10.1364/AO.20.000177.

Steeman-Nielsen, E., 1952. The use of radio-active carbon (C^{14}) for measuring organic production in the sea. ICES J. Mar. Sci. 18, 117–140. http://dx.doi.org/10.1093/icesjms/18.2.117.

Straneo, F., Cenedese, C., 2015. The dynamics of Greenland's glacial fjords and their role in climate. Annu. Rev. Mar. Sci. 7, 89–112. http://dx.doi.org/10.1147/annurev-marine-010213-135133.

Straneo, F., Heimbach, P., 2013. North atlantic warming and the retreat of Greenland's outlet glaciers. Nature 36, 504. http://dx.doi.org/10.1038/nature12854.

Stuart-Lee, A.E., Mortensen, J., Kaaden, A.S., Meire, L., 2021. Seasonal hydrography of Ameralik: A southwest Greenland fjord impacted by a land-terminating Glacier. J. Geophys. Res. 126, http://dx.doi.org/10.1029/2021JC017552.

Vonnahme, T.R., Persson, E., Dietrich, U., Hejdukova, E., Dybwad, C., Elster, J., Chierici, M., Gradinger, R., 2021. Early spring subglacial discharge plumes fuel under-ice primary production at a Svalbard tidewater glacier. Cryosphere 15, 2083–2107. http://dx.doi.org/10.5194/tc-15-2083-2021.

Wood, M., Rignot, E., Fenty, I., L., An., Bjørk, A., Broeke, M., Cai, C., Kane, E., Menemenlls, D., Millan, R., Morlighem, M., Mouginot, J., Noël, B., Scheuchl, B., Vellcogna, I., Wills, J.K., Zhang, H., 2021. Ocean forcinn drives glavier retreat in Greenland. Sci. Adv. 7, eaba7282. http://dx.doi.org/10.1126/sciadv.aba7282.

Yde, J., Knudsen, N.T., Hasholt, B., Mikkelsen, A.B., 2014. Meltwater chemistry and solute export from a Greenland ice sheet catchment, Watson River, West Greenland. J. Hydrol. 519, 2165–2179. http://dx.doi.org/10.1016/j.jhydrol.2014.10.018.

Young, T.J., Christoffersen, P., Bougamont, M., Tulaczyk, S.M., Hubbard, B., Makoff, K.D., Nicholls, K.W., Stewart, C.L., 2022. Rapid basal melting of the Greenland ice sheet from surface meltwater drainage. Proc. Natl. Acad. Sci. USA 119, http://dx.doi.org/10.1073/pnas.2116036119.